



HAL
open science

High performance of variable-pitch wind system based on a direct matrix converter-fed DFIG using third order sliding mode control

Amal Dendouga, Abdelhakim Dendouga, Najib Essounbouli

► To cite this version:

Amal Dendouga, Abdelhakim Dendouga, Najib Essounbouli. High performance of variable-pitch wind system based on a direct matrix converter-fed DFIG using third order sliding mode control. *Wind Engineering*, 2023, 48 (3), pp.325-348. 10.1177/0309524X231199435 . hal-04297359

HAL Id: hal-04297359

<https://hal.science/hal-04297359v1>

Submitted on 26 Sep 2024


HAL is a multi-disciplinary open access archive for the deposit and dissemination of scientific research documents, whether they are published or not. The documents may come from teaching and research institutions in France or abroad, or from public or private research centers.

L'archive ouverte pluridisciplinaire **HAL**, est destinée au dépôt et à la diffusion de documents scientifiques de niveau recherche, publiés ou non, émanant des établissements d'enseignement et de recherche français ou étrangers, des laboratoires publics ou privés.



Distributed under a Creative Commons Attribution 4.0 International License

High performance of variable-pitch wind system based on a direct matrix converter-fed DFIG using third order sliding mode control

Wind Engineering
2024, Vol. 48(3) 325–348
© The Author(s) 2023
Article reuse guidelines:
sagepub.com/journals-permissions
DOI: 10.1177/0309524X231199435
journals.sagepub.com/home/wie


Amal Dendouga¹ , Abdelhakim Dendouga² and Najib Essounbouli³

Abstract

In this paper, a full nonlinear control of a variable-pitch wind system (VPWS) based on the doubly fed induction generator (DFIG) fed by a direct matrix converter (DMC) has been presented. In this context, The MPPT has been implemented using the third order sliding mode control (TOSMC) in order to ensure maximum power provided by the wind turbine on the one side, on the other side the pitch control has been implemented in order to limit the power extracted to its nominal value. Moreover, a TOSMC has been incorporated into the direct field-oriented control (DFOC) to ensure high-performance control of the active and reactive power of DFIG. To examine the performance of the TOSMC, a comparative study was performed between this last type and the first and second order sliding mode controllers. The obtained results affirmed the high performance provided by the TOSMC compared to lower order sliding mode controllers.

Keywords

Direct field-oriented control, direct matrix converter, doubly fed induction generator, Maximum Power Point Tracking, third order sliding mode control, variable-pitch wind system, pitch control

Introduction

Currently, wind energy is one of the most widely used renewable sources of electrical energy generation, due to its less damaging environmental influences and its inexhaustible source. During the last decades, wind power systems have undergone a swift development thanks to the considerable development in the field of power electronics and control strategies (Kaloï et al., 2016; Soomro et al., 2021).

The researchers have given great importance to the variable speed wind system compared to the fixed speed system due to its ability to operate under different wind speeds. Thus, the Maximum Power Point Tracking (MPPT) strategy can be applied to extract the maximum power from the wind turbine. In addition, the pitch angle control of the blades can be designed in order to protect the wind turbine from higher wind speeds (Dahbi et al., 2016).

In this context, the DFIG is quite popular in the variable speed wind energy conversion system because of its high performance, the possibility to control stator active and reactive powers, and the most important advantage of DFIG is that the operating in a wide speed range ($\pm 30\%$) this means reduced power converter size and reduced maintenance cost (Patel et al., 2021; Soomro et al., 2021).

Actually, the extensive development in the field of microelectronics and information technologies has allowed the appearance of new topologies of power converters more suitable for the supply of DFIG such as matrix

¹Laboratory of Energy Systems Modeling, Department of Electrical Engineering, University of Biskra, Biskra, Algeria

²3CUB Research Laboratory, Department of Electrical Engineering, University of Biskra, Biskra, Algeria

³CReSTIC IUT of Troyes, University of Reims Champagne-Ardenne, Troyes, France

Corresponding author:

Amal Dendouga, MSE Laboratory, Department of Electrical Engineering, University of Biskra, BP 145, Biskra 07000, Algeria.

Email: am.dendouga@univ-biskra.dz

converters instead of traditional indirect AC/DC/AC converters (Nguyen et al., 2020). Therefore, the DMC allows bi-directional power conversion between the DFIG and the grid without a DC link (Aydogmus et al., 2022; Dendouga and Dendouga, 2022).

To improve the input current waveform, therefore reducing the harmonic distortion rate THD of the input current in DMC, a passive filter must be connected between the DMC and the grid. Several passive filter topologies have been proposed in the research works; however, the passive filter with a damping resistor connected in parallel with the inductor has been considered a suitable solution (Dendouga, 2020; Dendouga and Dendouga, 2022).

According to the literature, Field Oriented Control (FOC) using PI controllers is the most popular method used to control the active and reactive power of DFIG-based WECS (Alhato and Bouallègue, 2019). It is very used due to its simplicity and reliability, but the main problem of this controller is the presence of a chattering phenomenon and a high THD of the current due to its linearity, especially during the rapid variation in wind speed.

For this reason, several studies have been performed to provide highly effective performances of control loops for the DFIG-based WECS; such as (Medjber et al., 2016) proposed neural networks and fuzzy logic controllers to control the active and reactive powers of DFIG, and the maximum power point tracking strategy is designed to extract the maximum power from the wind turbine. In El Mourabit et al. (2019), a nonlinear backstepping control is applied to a variable speed wind energy conversion system based on PMSG. A simulation using Matlab/Simulink and the control implementation in the DS1104R&D Controller Board for experimental validation are presented. Rezaei (2018) presented a nonlinear adaptive backstepping control method for MPPT of DFIG-based wind energy conversion systems. The laws of backstepping control do not require knowledge of the machine parametric characteristics. Taraft et al. (2015) proposed the sliding mode control (SMC) method to control active and reactive powers of DFIG supplied by matrix converter for wind turbine system. The Perturbation and Observation maximum power point tracking is designed to extract the maximum power from the wind turbine. Chojaa et al. (2021) proposed an integral sliding mode control (ISMC) to control the active and reactive powers of a doubly fed induction generator (DFIG) based wind turbine. And as well an artificial Neural Network Control (ANNC) was presented for maximum power point tracking in order to extract the maximum power. Kelkoul and Boumediene (2021) presented a nonlinear, super twisting sliding mode controller to control the active and reactive powers of DFIG-based WECS. The performance of the proposed technique was compared to that of the sliding mode controller in terms of parameter variations. In Dursun and Kulaksiz (2020), second-order Sliding mode control (SO-SMC) is designed to capture maximum power from the WECSs, it is validated by two different wind speed profiles. A comparative study between the proposed approach SOSMC and conventional SMC is presented.

In this paper, a full control of a variable-pitch wind system based on a direct matrix converter-fed DFIG is designed using TOSMC to improve performances of the system under the stochastic variations in the wind speed.

The current work examines three main topics:

The first topic was to design the MPPT strategy using the TOSMC to optimize the exploitation of wind energy. As well as, the pitch angle control technique based on the PI controller was applied when the wind speed exceeds its nominal value in order to limit the power extracted to its nominal value and also avoid malfunctioning of the system. The second topic was to show that a DMC structure can be used for a VPWS without DC-link problems. A DMC provides bidirectional power flow from the grid to DFIG or vice versa. The DMC needs an input filter to enhance the input current waveform and decrease the harmonics injected by the system into the grid; therefore, a damped RLC passive input filter topology was designed. A nonlinear control of active and reactive power of a DFIG using of the TOSMC in order to improve the performance and efficiency of the system was designed as the third topic of this work.

The overall structure of the paper is organized as follows: The mathematical modeling of wind turbine and of DFIG is provided briefly in section "Modeling of the variable-pitch wind system." Section "MPPT strategy with speed control" introduces the maximum power point tracking strategy with speed control, while the control of blade angle (pitch angle control) is described in section "Control of the blade angle." Section "Control of DFIG" includes the DFOC control scheme with designed controllers (PI, FOSMC, SOSMC, and TOSMC). Section "Venturini switching algorithm for DMC" describes Venturini switching algorithm for direct matrix converter. Damped passive input filter is designed in section "Damped passive RLC input filter." The simulation results with a comparative study are presented and discussed in section "Results and discussion." Finally, conclusions of this study are given in section "Conclusion."

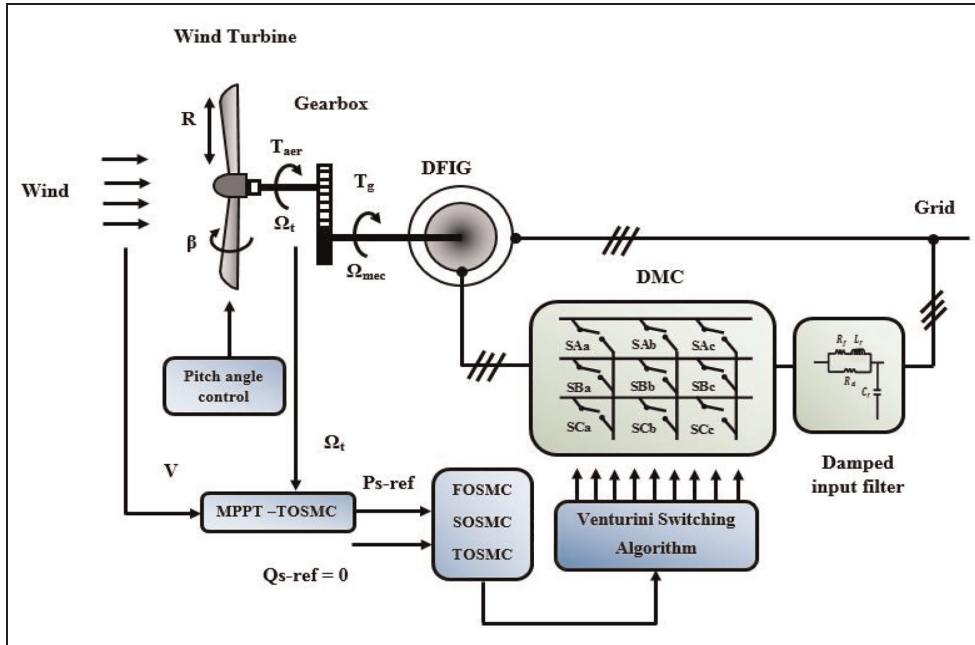


Figure 1. Descriptive diagram of the variable speed wind turbine system based on a DFIG.

Modeling of the variable-pitch wind system

The structure studied in this work is based on a variable-pitch wind system using a DFIG with Gearbox; the stator of the generator is connected directly to the grid, while the rotor is connected to the grid via a DMC. Figure 1 shows the structure of the whole system.

Model of wind turbine

When winds with speed V and air density ρ pass through a swept area by the blades S of a wind turbine, the wind power is (Khan, 2022; Soomro et al., 2021):

$$P_{wind} = \frac{1}{2} \rho s v^3 \quad (1)$$

The aerodynamic power generated by the wind turbine is related to the wind power through a power conversion coefficient C_p as follows (Khan, 2022; Wang et al., 2021):

$$P_{aer} = \frac{1}{2} \rho \pi R^2 v^3 C_p \quad (2)$$

The tip speed ratio λ is expressed by the following expression (Adouni et al., 2016; Kaloi et al., 2016):

$$\lambda = \frac{\Omega_t R}{v} \quad (3)$$

Where: ρ is the density of the air ($\rho \approx 1.22 \text{ kg/m}^3$ at atmospheric pressure at 20°C); S is the swept area by the wind turbine ($s = \pi R^2$); R is the blade length; V is the wind speed; and Ω_t is the angular speed of the wind turbine.

The power coefficient $C_p(\lambda, \beta)$ is a function of the pitch angle (β) and tip speed ratio (λ), which can be defined by the following equation (Amrane and Chaiba, 2016; Yaichi et al., 2019a):

$$C_p(\lambda, \beta) = (0.35 - 0.0167(\beta - 2)) \sin \left[\frac{\pi(\lambda + 0.1)}{14.43 - 0.3(\beta - 2)} \right] - 0.00184(\lambda - 3)(\beta - 2) \quad (4)$$

The aerodynamic torque imparted on the wind turbine is given by the equation (5)

$$T_{aer} = \frac{P_{aer}}{\Omega_t} = C_p(\lambda, \beta) \frac{\rho s v^3}{2} \frac{1}{\Omega_t} \quad (5)$$

The dynamic equation of the system can be written as follows (Chojaa et al., 2021; Kelkoul and Boumediene, 2021):

$$J \frac{d\Omega_{mec}}{dt} = T_g - T_{em} - f\Omega_{mec} \quad (6)$$

With:

$J = \frac{J_t}{G^2} + J_g$ is a total inertia of the wind turbine and generator, $f = \frac{f_t}{G^2} + f_g$ is a viscous total friction coefficient, $\Omega_{mec} = G \Omega_t$ is the rotation speed of the generator, $T_g = \frac{T_{aer}}{G}$ is the generator torque, G is the transmission ratio of the gearbox, and T_{em} is the electromagnetic torque of generator.

Model of DFIG

Due to the strongly coupled dynamics in DFIG, the modeling and control of DFIG in the three-phase system (abc) are quite difficult (Yaichi et al., 2019b; Sami et al., 2020).

Therefore, the dynamical model of the DFIG in the d, q Park reference frame is given by the following electrical equations (Amrane et al., 2022; Djilali et al., 2020):

$$\begin{aligned} v_{sd} &= R_s I_{sd} + \frac{d}{dt} \phi_{sd} - \omega_s \phi_{sq} \\ v_{sq} &= R_s I_{sq} + \frac{d}{dt} \phi_{sq} + \omega_s \phi_{sd} \\ v_{rd} &= R_r I_{rd} + \frac{d}{dt} \phi_{rd} - (\omega_s - \omega_r) \phi_{rq} \\ v_{rq} &= R_r I_{rq} + \frac{d}{dt} \phi_{rq} + (\omega_s - \omega_r) \phi_{rd} \end{aligned} \quad (7)$$

Where the expressions of flux are given by (Morshed and Fekih, 2017; Saihi et al., 2019):

$$\begin{aligned} \phi_{sd} &= L_s I_{sd} + M_{sr} I_{rd} \\ \phi_{sq} &= L_s I_{sq} + M_{sr} I_{rq} \\ \phi_{rd} &= L_r I_{rd} + M_{sr} I_{sd} \\ \phi_{rq} &= L_r I_{rq} + M_{sr} I_{sq} \end{aligned} \quad (8)$$

The expressions of active and reactive power can be given by equations (9) and (10) (Benbouhenni and Bizon, 2021b):

$$P_s = \frac{3}{2} (v_{sd} I_{sd} + v_{sq} I_{sq}) \quad (9)$$

$$Q_s = \frac{3}{2} (v_{sq} I_{sd} - v_{sd} I_{sq}) \quad (10)$$

The electromagnetic torque is related to a stator flux and to a rotor currents as follows (Soomro et al., 2021):

$$T_{em} = \frac{3}{2} n_p \frac{M_{sr}}{L_s} (\phi_{sd} I_{rq} - \phi_{sq} I_{rd}) \quad (11)$$

Where: ω_s , ω_r are stator and rotor pulsation, R_s and R_r are the stator and rotor resistances, L_s and L_r are stator and rotor inductances, M_{sr} is mutual inductance and n_p is the number of pole pairs.

The C_p value is proportional to the tip speed ratio λ , Figure 2 shows the variation of C_p under different pitch angles β .

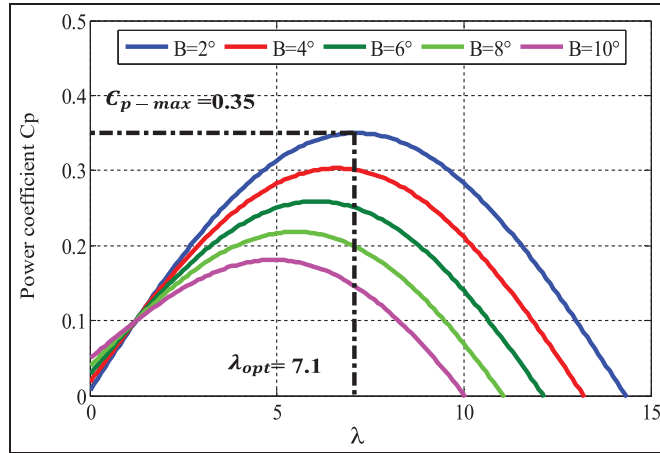


Figure 2. Power coefficient $C_p(\lambda, \beta)$ curves for several values of pitch angles β .

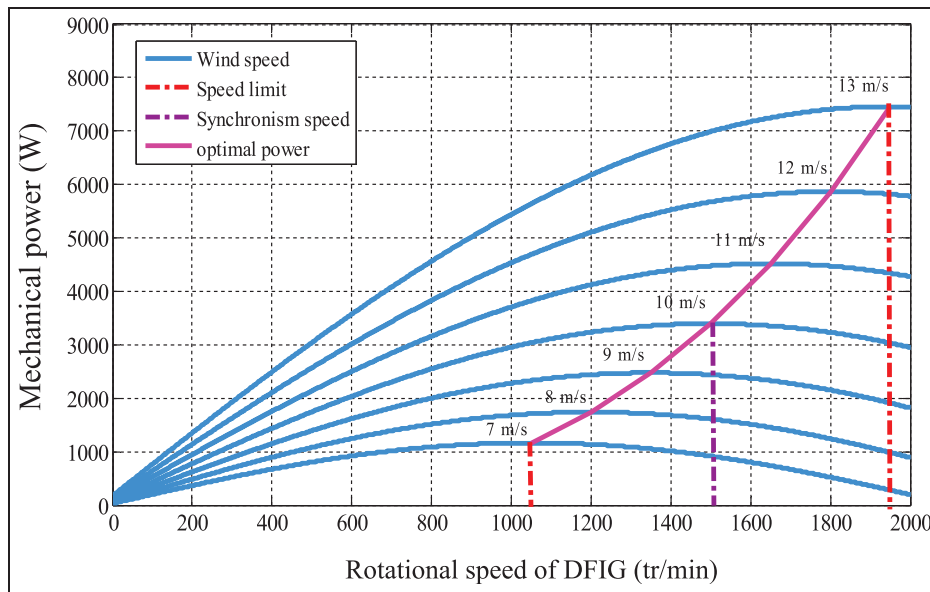


Figure 3. Power characteristics of VPWS under different values of wind speeds.

From Figure 2 it can be seen that, the power coefficient reaches the maximum value $C_{p_max} = 0.35$ at the optimal tip speed ratio $\lambda_{opt} = 7.1$ which corresponds to $\beta = 2^\circ$.

Figure 3 illustrates the $P_{mec} - \Omega_{mec}$ curve of the wind turbine under different wind speeds. From this figure, it is clear that for each wind speed, there is a maximum mechanical power captured by the wind turbine. The intersection points of the pink line with every curve present the maximum power that has to be extracted from the wind turbine to achieve the optimum operating point continuously.

The tracking of a maximum power point of a wind turbine may encounter some problems so, our purpose is the application of the MPPT strategy with different controllers for tracking the maximum power of a wind turbine under different wind speeds.

According to the wind speed, two techniques of control are distinguished: the first is the maximum power point tracking (MPPT) technique to maximize the extracted power, and the second is the pitch angle control technique in order to limit the mechanical power to its nominal value when the wind speed exceeds its nominal value.

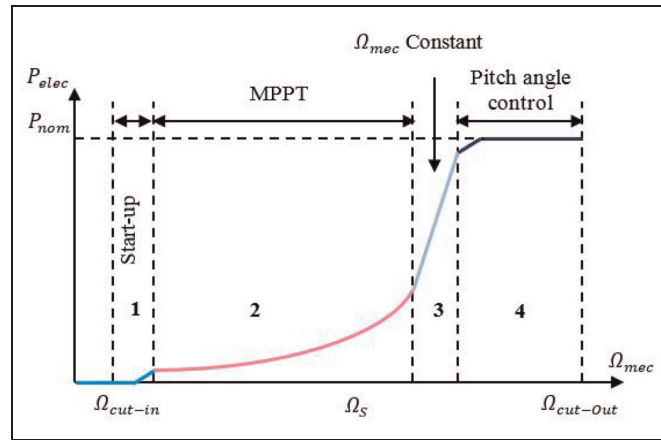


Figure 4. VPWS operating zones.

MPPT strategy with speed control

The MPPT strategy is designed in the WEC system as an optimization solution that aims to enhance the efficiency of the VPWS by exploiting the maximum energy from the wind whatever the wind speed; it involves the ongoing search for the maximum power from the wind when the available power is lower than the nominal generator power (Dahbi et al., 2016). This is obtained if the power coefficient C_p is at its maximum value by adjusting the mechanical speed Ω at the reference which corresponds to an optimum value Figure 4 (Zone II) (Medjber et al., 2016).

To achieve this step, the expression of reference speed is set at the maximum value given by (Hamzaoui et al., 2016):

$$\Omega_{t-ref} = \frac{v\lambda_{opt}}{R} \tag{12}$$

And the maximum value of power is written as follows (Dahbi et al., 2016):

$$P_{aer} = \frac{1}{2} \rho s C_{p-max}(\lambda_{opt}, \beta) \left(\frac{R\Omega_{t-ref}}{\lambda_{opt}} \right)^3 \tag{13}$$

The expression of reference electromagnetic torque is as follows:

$$T_{em-ref} = C_{\Omega}(\Omega_{mec-ref} - \Omega_{mec}) \tag{14}$$

With:

C_{Ω} is the controller of speed, T_{em-ref} is the reference electromagnetic torque, $\Omega_{mec-ref} = G\Omega_{t-ref}$.

The MPPT strategy with speed control is represented in the form of a simplified block diagram given in Figure 5.

In this paper, three types of controllers are studied to control the mechanical speed in order to follow its reference such as first order sliding mode control FOSMC, second order sliding mode control SOSMC based on a super twisting algorithm STA, and third order sliding mode control TOSMC.

First order sliding mode controller FOSMC

Sliding mode control is a nonlinear control method developed to control the mechanical speed of the wind turbine due to its simplicity and robustness; where its structure consists of two parts, one concerning the equivalent control (u_{eq}) and the other the switching component (u_n) (Dursun and Kulaksiz, 2020).

The principle of this method depends on keeping the system states on the sliding surface to achieve the stability of a system.

Consider the following sliding surface of mechanical speed:

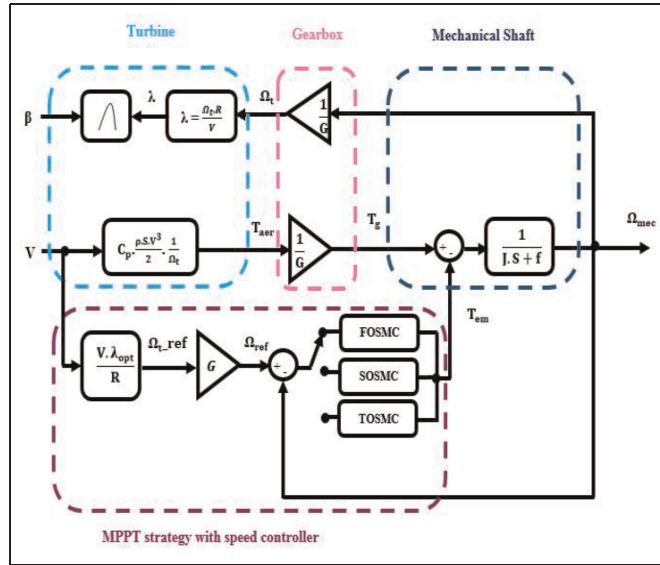


Figure 5. Scheme of MPPT strategy with speed control.

$$S_{\Omega_{mec}} = \Omega_{mec_ref} - \Omega_{mec} \tag{15}$$

The derivative of equation (15) is deduced as follows:

$$\dot{S}_{\Omega_{mec}} = \dot{\Omega}_{mec_ref} - \frac{1}{J}(T_g - T_{em} - f\Omega_{mec}) \tag{16}$$

According to equation (16), the expression of reference electromagnetic torque is:

$$T_{em_ref} = T_{em_eq} + T_{em_n} \tag{17}$$

Where T_{em_eq} and T_{em_n} are the equivalent and switching components of the control, respectively.

During the sliding mode and in permanent mode, we have $S_{\dot{\Omega}_{mec}} = 0$ (Dendouga, 2020).

From equation (16), the expression of equivalent component is obtained as follows:

$$T_{em_eq} = T_g - J\dot{\Omega}_{mec_ref} - f\Omega_{mec} \tag{18}$$

The switching component is adopted as:

$$T_{em_n} = K_{\Omega_{mec}} \text{sign}(S_{\Omega_{mec}}) \tag{19}$$

Thus, the total control T_{em_ref} is expressed by:

$$T_{em_ref} = T_g - J\dot{\Omega}_{mec_ref} - f\Omega_{mec} + K_{\Omega_{mec}} \text{sign}(S_{\Omega_{mec}}) \tag{20}$$

In the convergence mode, consider the following the Lyapunov function (Taraft et al., 2015; Yaichi et al., 2019):

$$\dot{V} = S_{mec} \dot{S}_{mec} < 0 \tag{21}$$

Equation (22) is considered

$$\dot{S}_{\Omega_{mec}} = \frac{K}{J} K_{\Omega_{mec}} \text{sign}(S_{\Omega_{mec}}) \tag{22}$$

The $K_{\dot{\Omega}_{mec}}$ must be negative.

Second order sliding mode controller SOSMC

To ensure good tracking and accurate response the second order sliding mode control SOSMC is designed. The super twisting algorithm STA insures all the properties of first order sliding mode control and reduces chattering in the system.

The second derivative of the sliding surface of mechanical speed $S_{\dot{\Omega}_{mec}}$ gives (Djilali et al., 2020):

$$\ddot{S}_{\Omega_{mec}} = G_1 + G_2 \dot{T}_{em_ref} \quad (23)$$

Where: $|G_1| \leq C$, $C > 0$, $0 < K_m \leq G_2 \leq K_M$.

According to the STA algorithm, the expression of the reference control variable T_{em_ST} is defined by the following equation (Borlaug, 2017; Dendouga, 2020):

$$T_{em_ST} = K_1 |S_{\Omega_{mec}}|^{0.5} \text{sign}(S_{\Omega_{mec}}) + K_2 \int \text{sign}(S_{\Omega_{mec}}) dt \quad (24)$$

Where K_1 and K_2 are determined according to the inequalities presented as follows (Dendouga, 2020; Djilali et al., 2020):

$$K_1^2 \geq \frac{4C K_M (K_2 + C)}{k_m^2 K_m (K_2 - C)}, K_2 > \frac{C}{K_m} \quad (25)$$

K_1 and K_2 are negative constants when the Lyapunov condition is verified ($\dot{V} = S_{mec} \dot{S}_{mec} < 0$). The reference torque is expressed by:

$$T_{em_ref} = T_{em_eq} + T_{em_ST} \quad (26)$$

Where: T_{em_eq} is the same obtained by equation (18).

Third order sliding mode controller TOSMC

To overcome the main drawbacks of FOSMC and SOSMC (the chattering phenomena and the ripples); the TOSMC was proposed (Borlaug, 2017). The TOSMC method is one of the nonlinear methods that have been suggested for controlling electrical systems (Benbouhenni and Bizon, 2021; Borlaug, 2017). As it can be used in the case of linear and non-linear systems due to the simplicity of its algorithm.

The control law of the proposed control TOSMC is given as follows:

$$\begin{aligned} U_{TOSMC} &= U_{ST} + U_{eq} + U_3 \\ U_{ST} &= U_1 + U_2 \end{aligned} \quad (27)$$

With:

$$\begin{aligned} U_1 &= K_1 |S|^{0.5} \text{sign}(S) \\ U_2 &= K_2 \text{sign}(S) \\ U_3 &= K_3 \int \text{sign}(S) dt \end{aligned}$$

In this paper, the TOSMC is used to force the mechanical speed to track its reference, the sliding surface of the mechanical speed $S_{\Omega_{mec}}$ is defined as the error between the desired and real value, as expressed in the following equation:

$$S_{\Omega_{mec}} = \Omega_{mec_ref} - \Omega_{mec} \quad (28)$$

The output signal for the mechanical speed controller is given as follows:

$$T_{em_TOSMC} = K_1 |S_{\Omega_{mec}}|^{0.5} \text{sign}(S_{\Omega_{mec}}) + K_2 \text{sign}(S_{\Omega_{mec}}) + K_3 \int \text{sign}(S_{\Omega_{mec}}) dt + T_{em_eq} \quad (29)$$

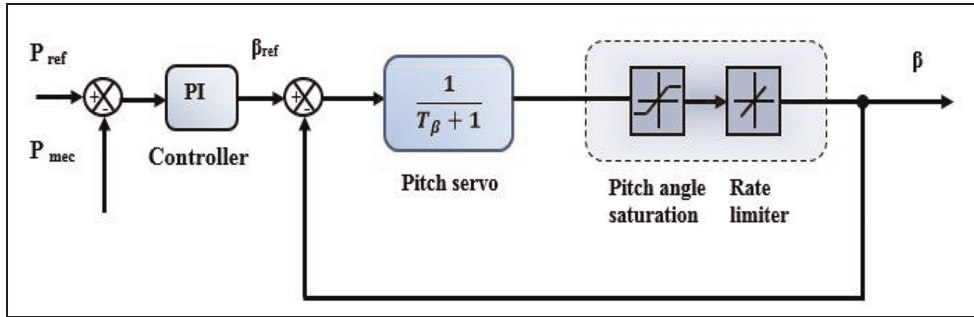


Figure 6. Scheme of pitch angle control strategy.

Where:

The expression of T_{em_eq} is the same given by equation (18).

The constants K_1 , K_2 , and K_3 are used to enhance the performance of the TOSMC controller.

To guarantee the stability condition, the Lyapunov equation must be satisfied (Dendouga, 2020):

$$\dot{v} = S_{\Omega_{mec}} \dot{S}_{\Omega_{mec}} < 0 \quad (30)$$

Control of the blade angle

The gusts of wind with a speed higher than its rated value can damage the wind energy conversion system. Therefore, it is necessary to use the pitch angle control of blades to protect the wind turbine from high power by limiting the power at its nominal value (Dahbi et al., 2016; Hamzaoui et al., 2016). The block diagram of pitch control is shown in Figure 6.

The principle of Pitch angle control is based on comparing the generated power from the wind turbine with the reference power, after that the error between them is sent to the PI controller which generates in the output reference value of the angle β ref.

The following equation expresses the relationship between the pitch angle β and its reference value β ref:

$$\beta = \frac{1}{\tau_{pitch} S} \beta_{ref} \quad (31)$$

With:

τ_{pitch} : is a time constant.

Control of DFIG

Direct field-oriented control DFOC

DFOC is one of the most widely strategies to control the DFIG, especially in industrial applications. The objective of this strategy is to control the DFIG in a way that makes its behavior similar to that of the DC motor with separate excitation (Benbouhenni and Bizon, 2021; Taraft et al., 2015).

The principle of a DFOC strategy depends on orienting the stator flux along the d axis, to simplify the control of stator power as follows (Benamor et al., 2019; Benbouhenni and Bizon, 2021):

$$\phi_{sd} = \phi_s \text{ and } \phi_{sq} = 0 \quad (32)$$

Hence, direct and quadrature stator voltages can be expressed as:

$$v_{sd} = 0 \text{ and } v_{sq} = v_s = \omega_s \phi_s \quad (33)$$

After simplifications, the expressions of stator current of the DFIG are given by:

$$\begin{cases} I_{sd} = \frac{v_s}{\omega_s L_s} \frac{M_{sr}}{L_s} I_{rd} \\ I_{sq} = -\frac{M_{sr}}{L_s} I_{rq} \end{cases} \quad (34)$$

The expression of stator active and reactive powers are given by (Dekali et al., 2021):

$$\begin{cases} P_s = -\frac{3}{2} v_s \frac{M_{sr}}{L_s} I_{rq} \\ Q_s = \frac{3}{2} \left(\frac{v_s^2}{\omega_s L_s} - v_s \frac{M_{sr}}{L_s} I_{rd} \right) \end{cases} \quad (35)$$

The equation (36) represent the electromagnetic torque.

$$T_{em} = -\frac{3}{2} n_p \frac{M_{sr}}{L_s} \phi_{sd} I_{rq} \quad (36)$$

The expressions of direct rotor voltage and quadrature rotor voltage of the DFIG are given by the following equations (Dekali et al., 2021):

$$\begin{cases} V_{rd} = R_r I_{rd} + L_r \sigma \frac{d}{dt} I_{rd} - g \omega_s L_r \sigma I_{rq} \\ V_{rq} = R_r I_{rq} + L_r \sigma \frac{d}{dt} I_{rq} + g \omega_s L_r \sigma I_{rd} + \frac{v_s M_{sr}}{L_s} \end{cases} \quad (37)$$

Where:

$\sigma = 1 - \frac{M_{sr}}{L_r L_s}$ is the dispersion coefficient of the DFIG, $g = \frac{\omega_s - \omega_r}{\omega_s}$ is the slip.

First order sliding mode control (FOSMC)

In order to track the stator powers of DFIG to their references, the sliding surface of stator active and reactive powers are expressed by (Boumar et al., 2019; Yaichi et al., 2019):

$$\begin{cases} S(P_s) = P_{s-ref} - P_s \\ S(Q_s) = Q_{s-ref} - Q_s \end{cases} \quad (38)$$

The derivative of (38) are given by (Boumar et al., 2019; Benbouzid et al., 2014):

$$\begin{cases} \dot{S}_{P_s} = \dot{P}_{s-ref} + \frac{3}{2} V_s \frac{M_{sr}}{L_s L_r \sigma} (V_{rq} - R_r I_{rq}) \\ \dot{S}_{Q_s} = \dot{Q}_{s-ref} + \frac{3}{2} V_s \frac{M_{sr}}{L_s L_r \sigma} (V_{rd} - R_r I_{rd}) \end{cases} \quad (39)$$

(39)

The expression of reference control variable is (Benbouzid et al., 2014; Dendouga, 2020):

$$V_{r,d,q} = V_{r,d,q,eq} + V_{r,d,q,n} \quad (40)$$

In steady state, $\dot{S}_{P_s} = 0$ and $\dot{S}_{Q_s} = 0$ (Dendouga, 2020).

The equivalent voltage component of control will be as follow:

$$\begin{cases} V_{rq,eq} = R_r I_{rq} - \frac{2}{3} P_{s-ref} \frac{L_s L_r \sigma}{V_s M_{sr}} \\ V_{rd,eq} = R_r I_{rd} - \frac{2}{3} Q_{s-ref} \frac{L_s L_r \sigma}{V_s M_{sr}} \end{cases} \quad (41)$$

The switching component is given by:

$$\begin{cases} V_{rq,n} = K_{P_s} \text{sign}(S_{P_s}) \\ V_{rd,n} = K_{Q_s} \text{sign}(S_{Q_s}) \end{cases} \quad (42)$$

Finally, the total control is written as follows:

$$\begin{cases} V_{rq,ref} = R_r I_{rq} - \frac{2}{3} \dot{P}_{s-ref} \frac{L_s L_r \sigma}{V_s M_{sr}} + K_{P_s} \text{sign}(S_{P_s}) \\ V_{rd,ref} = R_r I_{rd} - \frac{2}{3} \dot{Q}_{s-ref} \frac{L_s L_r \sigma}{V_s M_{sr}} + K_{Q_s} \text{sign}(S_{Q_s}) \end{cases} \quad (43)$$

The Lyapunov equation can be given as follows (Bounar et al., 2019):

$$\dot{v} = S_{P_s, Q_s} \dot{S}_{P_s, Q_s} < 0 \quad (44)$$

The conditions (41) are satisfied when:

$$\text{If } \text{sign}(S_{P_s, Q_s}) > 0 \dot{S}_{P_s, Q_s} < 0 \quad (45)$$

$$\text{If } \text{sign}(S_{P_s, Q_s}) < 0 \dot{S}_{P_s, Q_s} > 0 \quad (46)$$

Thus, K_{P_s} and K_{Q_s} must be positive.

Second order sliding mode control (SOSMC)

Equation (47) give the second derivative of the sliding surface of stator powers S_{P_s} and S_{Q_s} (Benbouzid et al., 2014; Djilali et al., 2020):

$$\begin{cases} \ddot{S}_{P_s} = G_1 + G_2 \dot{V}_{rq_ref} \\ \ddot{S}_{Q_s} = G_1 + G_2 \dot{V}_{rd_ref} \end{cases} \quad (47)$$

Where: $|G_1| \leq C$, $C > 0$, $0 < K_m \leq G_2 \leq K_M$.

When the STA algorithm is applied, the reference control variable of the stator powers is written as in the following equations (Dendouga, 2020; Kelkoul and Boumediene, 2021):

$$\begin{cases} V_{rqST} = K_1 |S_{P_s}|^{0.5} \text{sign}(S_{P_s}) + K_2 \int \text{sign}(S_{P_s}) dt \\ V_{rdST} = K_1 |S_{Q_s}|^{0.5} \text{sign}(S_{Q_s}) + K_2 \int \text{sign}(S_{Q_s}) dt \end{cases} \quad (48)$$

Where K_1 and K_2 are:

$$K_1^2 \geq \frac{4C K_M (K_2 + C)}{k_m^2 K_m (K_2 - C)}, K_2 > \frac{C}{K_m} \quad (49)$$

K_1 and K_2 are positive constants when the Lyapunov condition is verified.

Equation (50) give the expression of the reference voltages generated by the second order sliding regulator as follows:

$$\begin{cases} V_{rqref} = V_{rqeq} + V_{rqST} \\ V_{rdref} = V_{rd eq} + V_{rdST} \end{cases} \quad (50)$$

Where: $V_{rd eq}$ and $V_{rq eq}$ are expressed by the same obtained in equation (41).

Third order sliding mode control (TOSMC)

Between different techniques of control used to improve the performances of the system (chattering reduction, tracking and robustness), the third order sliding mode control TOSMC is proposed to control the stator powers.

Equation (51) give the sliding surface of the stator active and reactive powers, which are selected as the error between the desired and real dynamics as follows (Benbouhenni and Bizon, 2021):

$$\begin{cases} S(P_s) = P_{s_ref} - P_s \\ S(Q_s) = Q_{s_ref} - Q_s \end{cases} \quad (51)$$

From equation (28), it can be deduced that the control laws applied to control the stator powers are expressed by the reference rotor voltage components as follows (Benbouhenni and Bizon, 2021; Borlaug, 2017):

$$\begin{cases} V_{rqref} = K_1 |S_{P_s}|^{0.5} \text{sign}(S_{P_s}) + K_2 \int \text{sign}(S_{P_s}) dt + K_{P_s} \text{sign}(S_{P_s}) + V_{rqeq} \\ V_{rdref} = K_1 |S_{Q_s}|^{0.5} \text{sign}(S_{Q_s}) + K_2 \int \text{sign}(S_{Q_s}) dt + K_{Q_s} \text{sign}(S_{Q_s}) + V_{rd eq} \end{cases} \quad (52)$$

The expressions of $V_{rd_{eq}}$ and $V_{rq_{eq}}$ are the same given by equation (41).

To guarantee the stability condition, the Lyapunov equation must be verified:

$$\dot{v} = S_{P_s, Q_s} \dot{S}_{P_s, Q_s} < 0 \quad (53)$$

Thus the constants K_1 , K_2 , and K_3 are positive.

Venturini switching algorithm for DMC

In this section, the Venturini switching algorithm for the DMC will be presented. In the power electronic laws the voltage sources must never be in a short and the current sources must never be in an open circuit (Dendouga, 2020), therefore possesses 27 possible combinations of switching for DMC (Dendouga and Dendouga, 2019).

The conduction time t_{ij} of the switch defined by (Dendouga, 2010):

$$t_{Aj} + t_{Bj} + t_{Cj} = T_{seq} \quad (54)$$

With: T_{seq} the switching sequence of the MC, and $0 < t_{ij} < T_{seq}$.

The duty cycle can be defined as (Hamane et al., 2015):

$$m_{ij}(t) = \frac{t_{ij}}{T_{seq}} \quad \text{where: } 0 < m_{ij} < 1$$

According to equation (54) one can give (Casadei et al., 2002):

$$m_{Aj} + m_{Bj} + m_{Cj} = 1 \quad (55)$$

Considering the ratio between the output voltage and the input voltage of the DMC (Chaoui et al., 2016; Hamane et al., 2015).

$$q = \frac{v_o}{v_i} = \frac{i_i}{i_o} \quad (56)$$

Furthermore, suppose that the desired output voltage is expressed by (Hamane et al., 2015):

$$V_o(t) = qV_{im} \begin{bmatrix} \cos(w_o t) \\ \cos(w_o t + \frac{2\pi}{3}) \\ \cos(w_o t + \frac{4\pi}{3}) \end{bmatrix} \quad (57)$$

From Venturini and Alesina (1980) the expression of the modulation matrix m is given by (Casadei et al., 2002; Rodríguez et al., 2005):

$$m_{ij} = \frac{1}{3} \left[1 + \frac{2V_i V_j}{V_{im}^2} \right] \quad (58)$$

Damped passive RLC input filter

The input passive filter is an essential component must be placed between the DMC and the grid to generate sinusoidal input currents, to therefore reduce the harmonic distortion rate.

In this paper, the passive filter with a damping resistor connected in parallel with the inductor proposed to increase the damping factor of the LC filter illustrated by Figure 7 (Nguyen et al., 2016).

The voltage and current transfer function of the input filter are given by the following expressions by (Dendouga, 2020; She et al., 2010):

$$\begin{cases} V_A(S) = \frac{(L_f S + R_d + R_f)V_{gd}(S) - R_d(L_f S + R_f)I_s(S)}{R_d L_f C_f S^2 + (R_d R_f C_f + L_f)S + (R_d + R_f)} \\ I_{gd}(S) = \frac{(L_f C_f S^2 + (R_d + R_f)C_f S)V_{gd}(S) + (L_f S + R_d + R_f)I_s(S)}{R_d L_f C_f S^2 + (R_d R_f C_f + L_f)S + (R_d + R_f)} \end{cases} \quad (59)$$

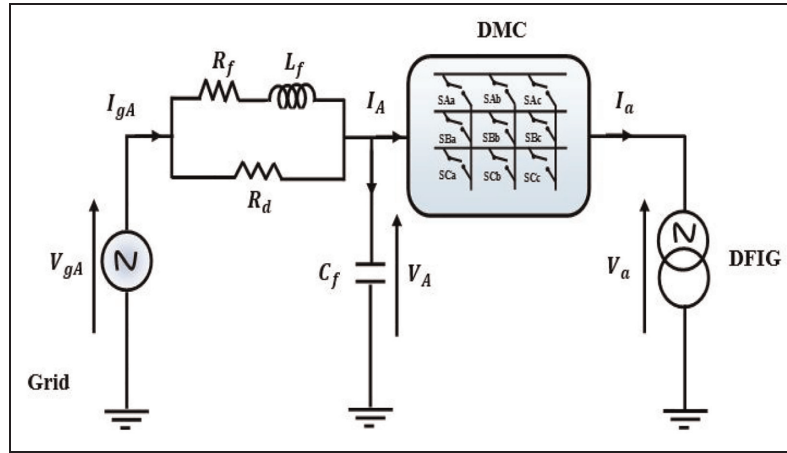


Figure 7. Single-phase circuit of damped input filter RLC for DMC.

The characteristic frequency ξ and the damping factor ω_n of transfer functions are defined as follows (Dendouga, 2020; She et al., 2010):

$$\begin{cases} \omega_n = \sqrt{\frac{R_d + R_f}{R_d L_f C_f}} \\ \xi = \frac{R_d R_f C_f + L_f}{2\sqrt{R_d L_f C_f (R_d + R_f)}} \end{cases} \quad (60)$$

Considering that damping resistor $R_d \gg (R_d \rightarrow \infty)$, and as the resistance of the inductor R_f is usually few ohms; the expression (60) could be simplified as (Dendouga, 2020; She et al., 2010):

$$\begin{cases} \omega_n = \frac{1}{\sqrt{L_f C_f}} \\ \xi = \frac{1}{2R_d} \sqrt{\frac{L_f}{C_f}} \end{cases} \quad (61)$$

Results and discussion

The simulation of variable-pitch wind system (VPWS) based on DFIG is carried out using Matlab/Simulink to validate the performance of the proposed control strategy. Table 1 displays parameters of the DFIG-based VPWS.

In this study, the efficiency of DFIG-based VPWS is investigated under the following two cases:

- A. Operating of the variable-pitch wind system in zone 2;
- B. Operating of the variable-pitch wind system in all zones.

Simulation results of control of the variable-pitch wind system in zone 2

In this case, the simulation of the MPPT strategy was implemented to enhance the efficiency of the VPWS by exploiting the maximum energy from the wind. In order to validate the efficiency of the considered wind system with different proposed control strategies, a comparative study was carried out.

In this context, the pitch angle of the blades for the wind turbine is constant $\beta = 2^\circ$ in this case. Figure 8 shows the wind speed profile, which is a random profile changes between 8 and 13 m/s.

When the wind speed is less than the nominal wind speed, the MPPT control strategy is necessary to extract the maximum power from the wind turbine. According to Figure 9, the maximum value of power coefficient $c_p(\lambda, \beta)$ is approximately 0.35, which corresponds to the optimum value of the tip speed ratio $\lambda_{opt} = 7.1$ for a pitch angle $\beta = 2^\circ$ in spite of the sudden variations of the wind speed.

Table 1. VPWS-DFIG parameters.

Parameters of VPWS-DFIG	Value
Rated power P_n	7.5 kW
Number of pair of poles P	2
Stator rated voltage V_s	220/380 V
Rotor resistance R_r	0.62 Ω
Stator resistance R_s	0.45 Ω
Stator inductance L_s	0.084 H
rotor inductance L_r	0.081 H
Mutual inductance M_{sr}	0.078 H
Friction coefficient f_r	0.0054 $N.m.s^{-1}$
$P_{turbine}$	7.5 kW
Rotor radius R	2.25 m
Gearbox gain G	5
Stator rated frequency f_s	50 Hz

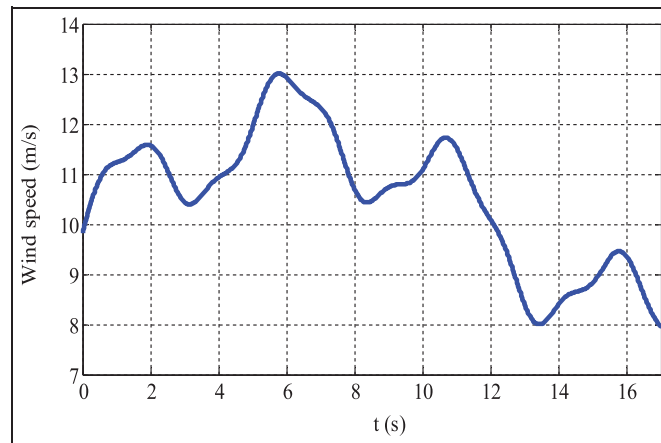


Figure 8. Random wind speed profile.

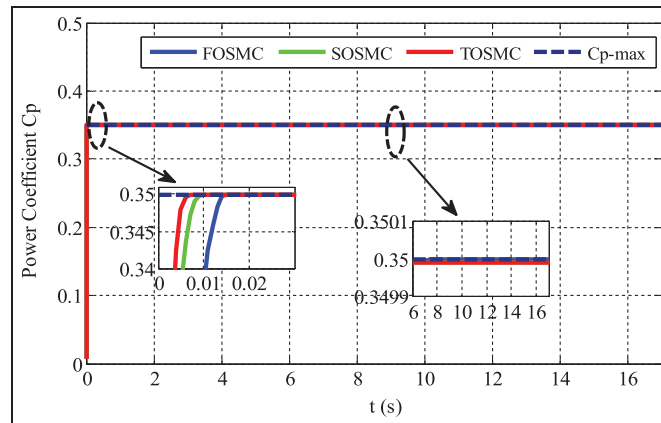


Figure 9. Represents the power coefficient in Zone 2.

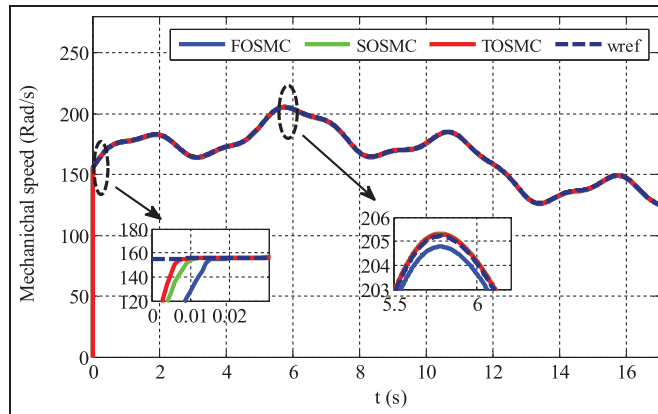


Figure 10. Represents the Rotor speed in Zone 2.

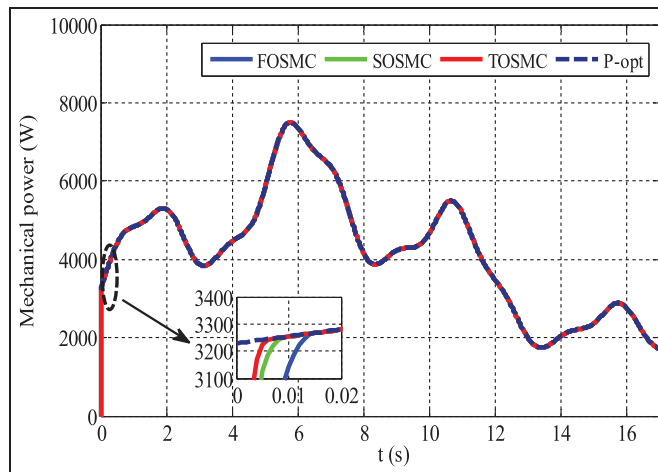


Figure 11. Represents the mechanical power in Zone 2.

The change of the power coefficient confirms that the three controllers tracked the maximum value $C_{p_{max}} = 0.35$. However, the TOSMC demonstrated faster response time and precision compared to the SOSMC and FOSMC.

The rotor speed of the turbine is shown in Figure 10 which is controlled in order to optimize the power in zone 2. It can be said that the speed is variable and takes the same shape as the wind speed change. As well the mechanical speed perfectly tracks its reference value for the three controllers, while the TOSMC has a fast response time compared to the other controllers.

Figure 11 shows the mechanical power generated by the turbine using three different types of controllers for the MPPT strategy, as it can be noted that all controllers attained the maximum exploitation of the power in spite of variations in the wind speed. However, the TOSMC has fast response time compared to the SOSMC and FOSMC.

Consequently, the obtained results clearly indicate the effectiveness of the dynamic performance of the TOSMC over the others controller under the stochastic variations of the wind speed.

Simulation results of full control of the variable-pitch wind system in all zones

In this case, the whole system of the variable-pitch wind energy system based on a doubly-fed induction generator fed by a direct matrix converter was carried out under MATLAB/Simulink environment.

The control system relies on the following approaches:

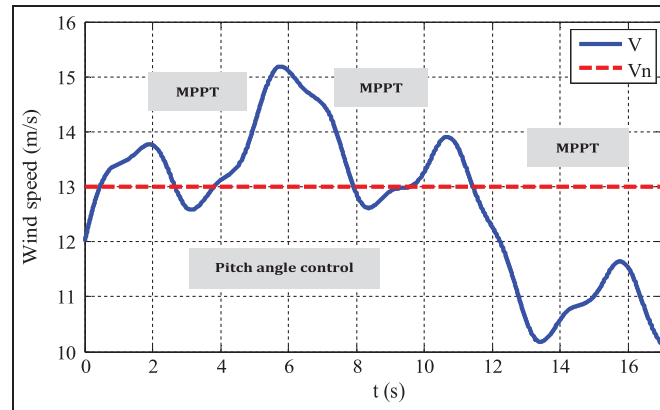


Figure 12. Random profile of high wind speed.

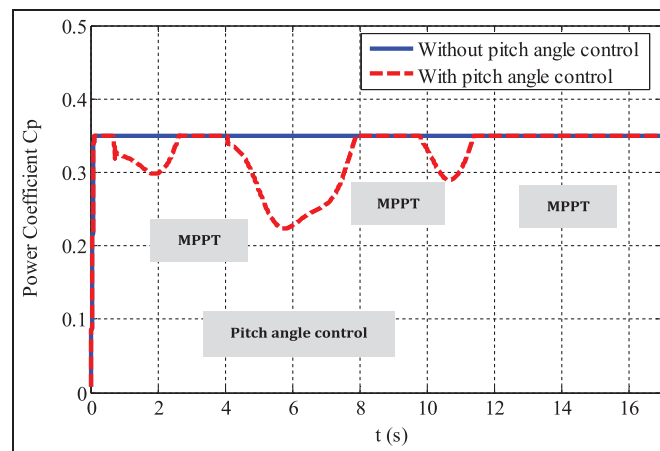


Figure 13. Represents the power coefficient in all Zones.

In the first approach, the MPPT strategy was proposed in order to extract the maximum power from the wind turbine when the wind speed is lower than the nominal speed on the one side. On the other side, the Pitch control was designed to adjust the blade angle so that the maximum rated power for the wind turbine is not exceeded. In this way, the protection of the system against high wind speeds is ensured. For this reason, a TOSMC controller was used to control the speed of the turbine due to its exceptional advantages compared to other controllers.

The second approach consists of the direct field-oriented control (DFOC) of active and reactive powers for the DFIG using third order sliding mode controller TOSMC, while controlling the direct matrix converter by Venturini modulation algorithm.

The following comparative study giving below were done to tests the robustness and performance of the proposed TOSMC controller under the stochastic variation of the wind speed.

In order to control the functioning of the wind turbine in the all zones of operating and validate the dynamic performances of the system studied, a random wind speed was applied, in which the wind speed profile simulated varies between 8 and 16 m/s as show Figure 12.

It can be seen clearly from Figure 13, that the power coefficient c_p attains its maximum value $c_{p_max} = 0.35$ with applied the MPPT strategy (Zone 2) when the wind speed is lower than the rated value ($V < V_n = 13$ m/s). While it decreases when the wind speed exceeds the rated speed ($V > V_n = 13$ m/s) by applying the pitch control technique (Zone 4).

Figure 14 illustrates the mechanical speed of the wind turbine which is controlled in order to maximize the power generated by the turbine using the MPPT strategy in Zone 2 and to be rated by applying the pitch control in Zone 4.

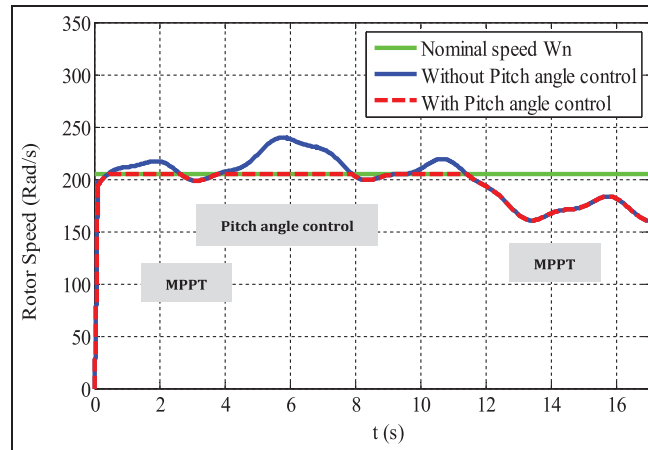


Figure 14. Represents the Rotor speed in all Zones.

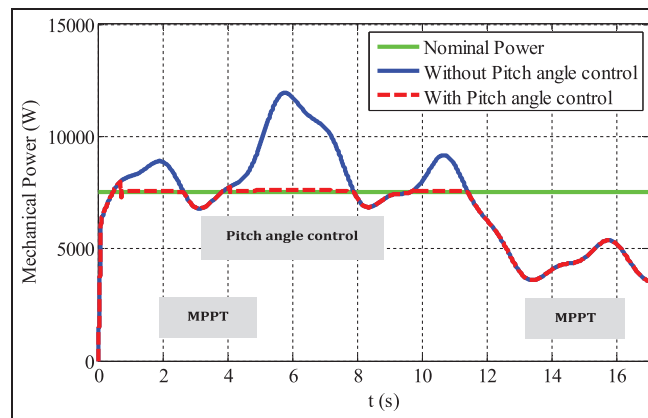


Figure 15. Represents the mechanical power in all Zones.

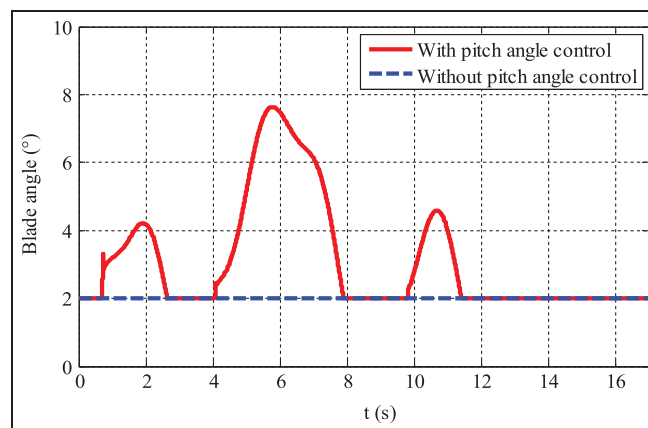


Figure 16. Pitch angle.

Figure 15 shows the power generated by the wind turbine. One can notice that the pitch angle control of the blades (β) intervenes (in Zone 4) when the wind speed is higher than the rated wind speed to limit the power to the nominal value (7.5 kW).

From Figure 16, one can show that the pitch angle value increases when the wind speed exceeds the rated value (13 m/s), in order to protect the wind turbine by limiting the generated power to its nominal value (7.5 kW). While, when the wind speed is lower than the rated wind speed the pitch angle value is equal 2°.

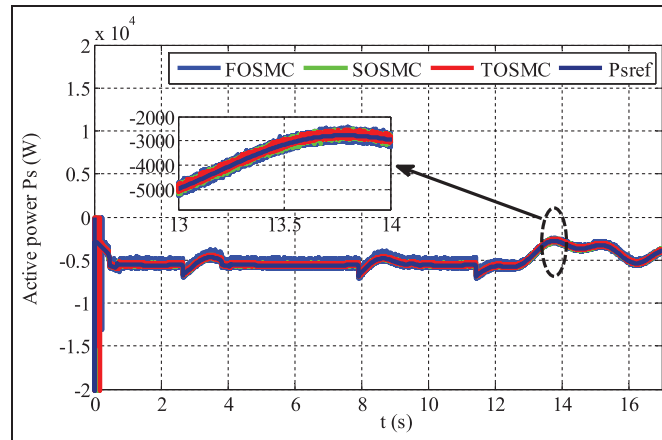


Figure 17. Stator active power of DFIG.

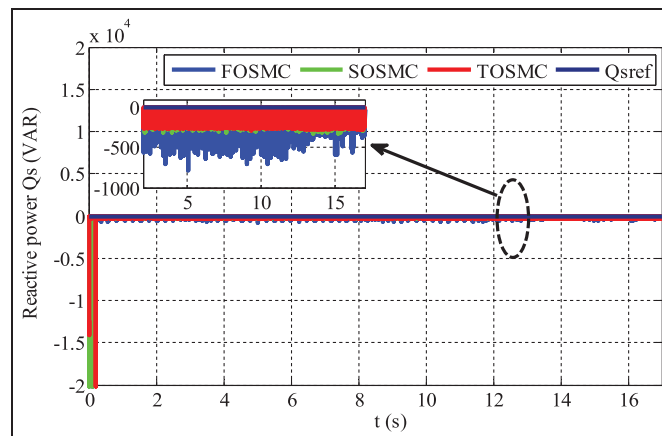


Figure 18. Stator reactive power of the DFIG.

The active and reactive powers generated by the DFIG are presented in Figures 17 and 18 respectively, the P_s and Q_s perfectly follow their references for the three controllers. While it can be seen that the TOSMC type controller gives good tracking of the stator powers to their references with low overshoot compared to FOSMC and SOSMC controllers with considerable overshoot for the different control modes (MPPT and Pitch Control). In order to optimize the quality of the electrical energy generated and to ensure operation with a unity power factor on the stator side, the reactive stator power Q_s is kept at null value ($Q_s = 0$ (VAR)). Additionally, the active power takes the same shape as the wind speed change, while the Q_s is not affected by the wind speed change.

The electromagnetic torque of the DFIG illustrates in Figure 19, for (FOSMC, SOSMC, and TOSMC controllers) and its reference obtained from the MPPT strategy based on TOSMC. It can be seen that the TOSMC makes it possible to obtain good tracking of the electromagnetic torque at its reference for the different modes of control (MPPT and Pitch Control).

From Figure 20, it can be seen that the waveform of rotor voltage per phase (at the output of the DMC) is formed by a succession of input voltage pulses (at the input of the DMC) by using a Venturini switching algorithm.

Figures 21 and 22 illustrate the stator current of DFIG and grid current, It can see that the three phases are sinusoidal with a frequency equal to $f = 50$ (Hz). However, the TOSMC controller improves the waveform compared to FOSMC and SOSMC controllers.

Figure 23 shows the THD of stator current obtained for the three controllers. It can see that the fundamental frequency is equal to 50 Hz and the THD is acceptable in the case of the TOSMC controller (1.06%; compliant with IEEE standard) compared to the other controllers: FOSMC (1.38%; compliant with IEEE standard) and

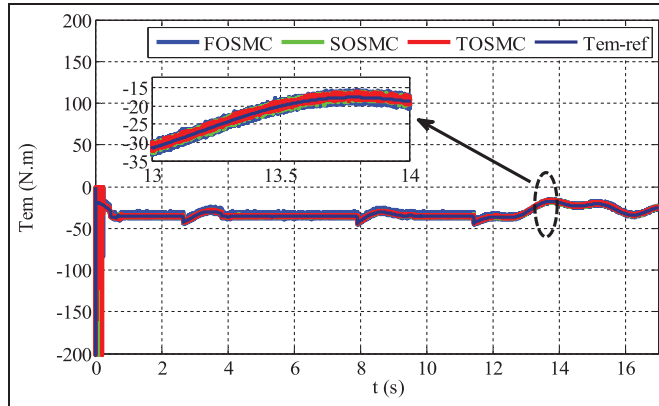


Figure 19. Electromagnetic torque of the DFIG.

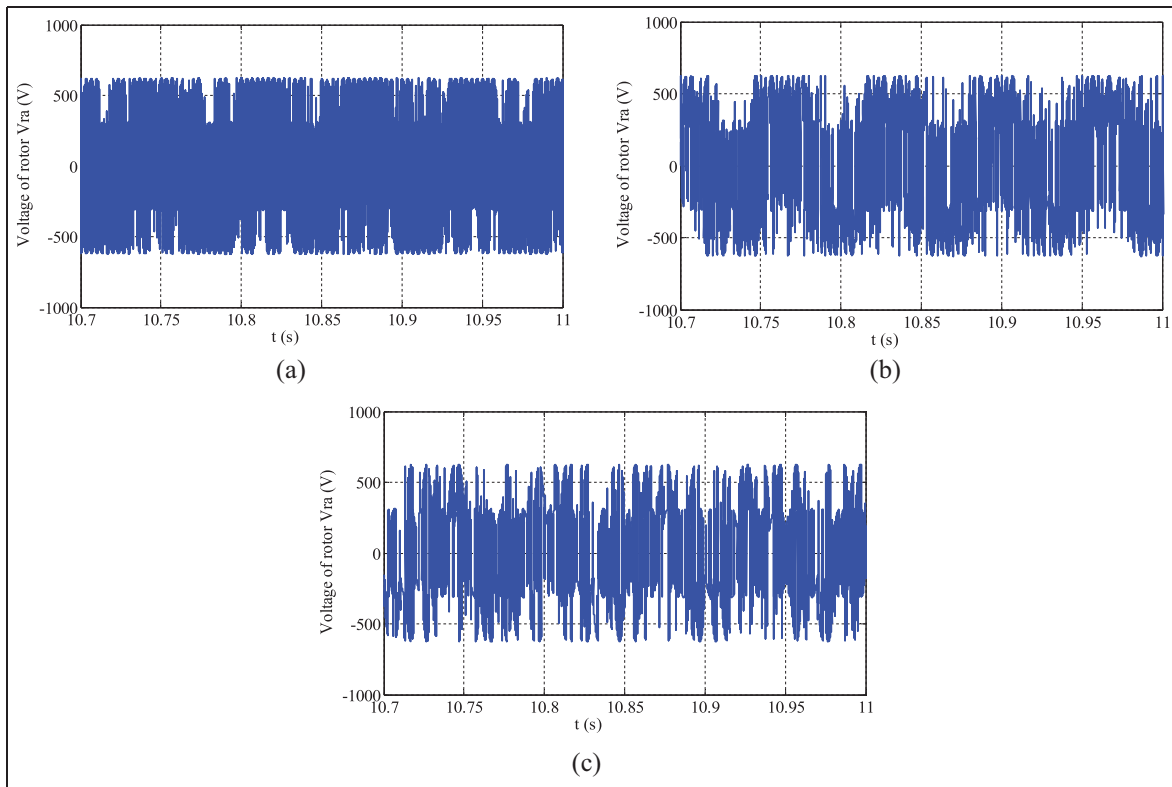


Figure 20. Rotor voltage V_{ra} : (a) FOSMC, (b) SOSMC, and (c) TOSMC.

SOSMC (1.28%; compliant with IEEE standard). Which makes it possible to inject clean energy with a low THD into the grid.

The waveform of the input current of the DMC illustrates in Figure 24, which is deduced by using the Venturini switching algorithm.

Table 2 presents a comparative summary of the proposed TOSMC strategy and others strategies used in this work.

According to the results illustrated in Table 2, it is confirmed that the TOSMC strategy is the most efficient in terms of good tracking and minimizing ripples of different curves (powers, electromagnetic torque, and stator currents) compared to the other strategies of control such as FOSMC and SOSMC. In addition, the TOSMC strategy

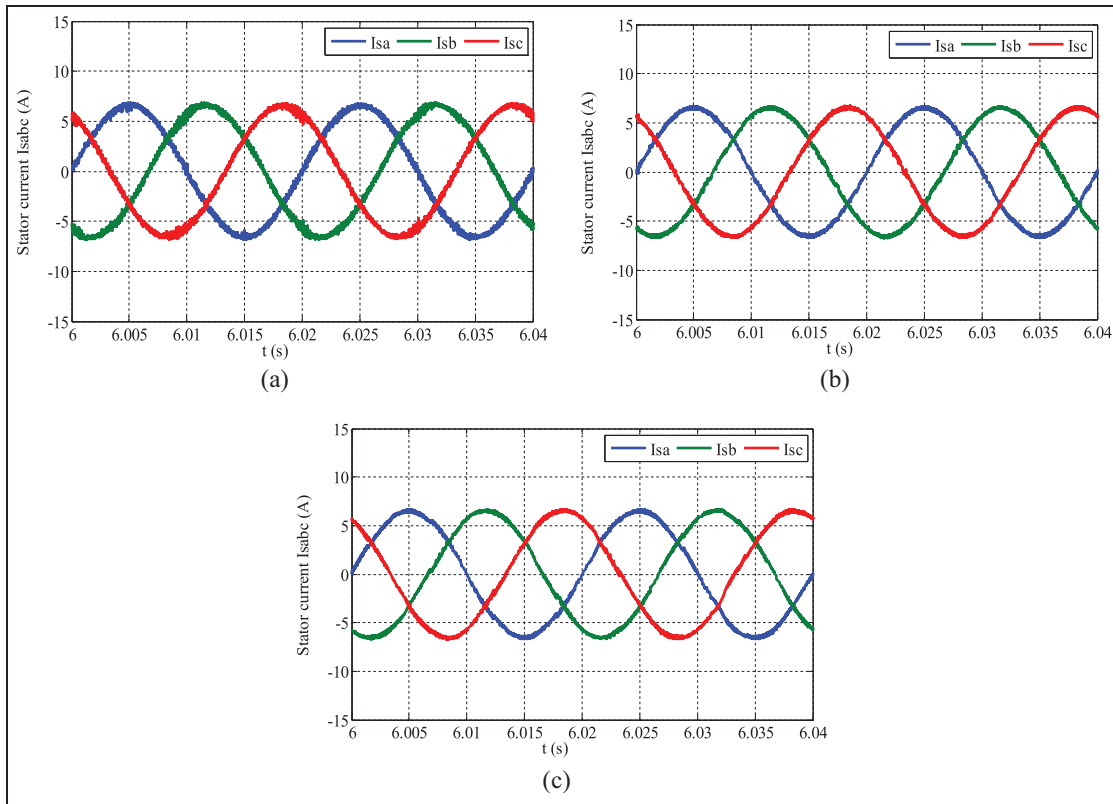


Figure 21. Stator currents I_s : (a) FOSMC, (b) SOSMC, and (c) TOSMC.

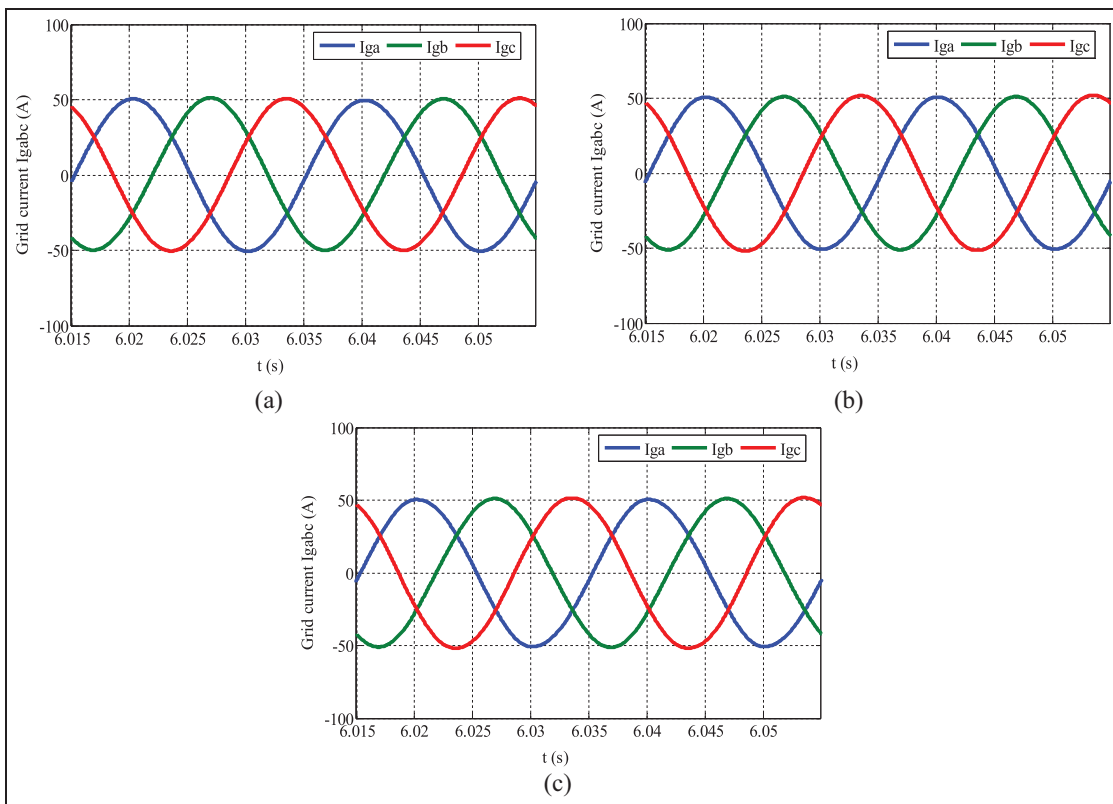


Figure 22. Grid currents: (a) FOSMC, (b) SOSMC, and (c) TOSMC.

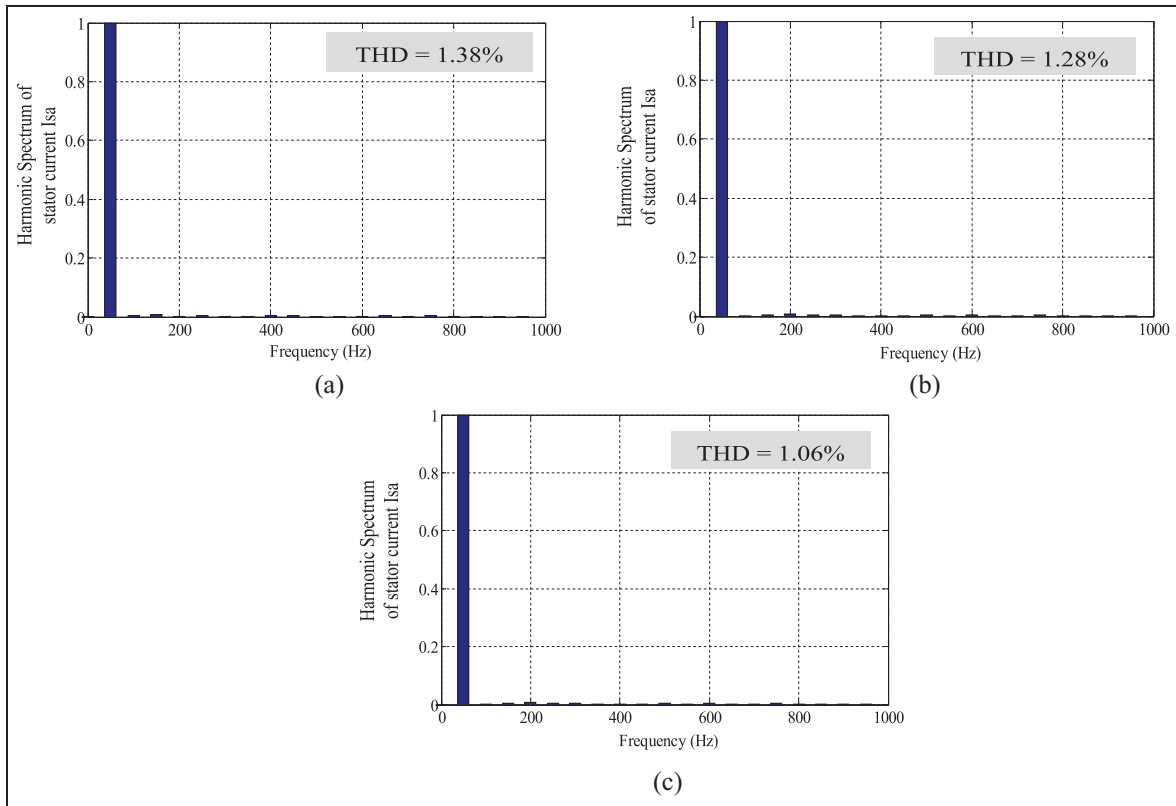


Figure 23. Harmonic spectrum of stator current: (a) FOSMC, (b) SOSMC, and (c) TOSMC.

ensures a good quality of power conversion between the DFIG and the grid with a reduced total harmonic distortion rate THD under the sudden variations in the wind speed.

Conclusion

This article deals with the development, design and implementation of the TOSMC strategy for the control of active and reactive powers generated by the variable pitch wind system based on DFIG.

In this context, full control of the wind turbine has been developed, as a first approach; the MPPT strategy based on a third-order sliding mode controller (TOSMC) has been designed in order to ensure maximum exploitation of the wind energy, and as a second approach; control of the pitch angle has been implemented in order to limit the power extracted to its maximum value for the safe operating of the system when the wind speed exceeded to the rated speed of the wind turbine.

In order to ensure direct energy conversion without needing a DC-link between the grid and the DFIG as in traditional power converters, a direct matrix converter controlled by the strategy of Venturini was proposed. Moreover, the RLC input passive filter with a damping resistor connected in parallel with the inductor was designed to obtain an almost sinusoidal waveform for the current with a low rate of total harmonic distortion (THD).

The TOSMC strategy has been tested and evaluated by comparing it with the other control techniques carried out using a random profile of the wind speed which changes between 8 and 16 m/s under Matlab/Simulink.

The simulation results demonstrate that the proposed TOSMC controller gives good performances compared to the FOSMC and SOSMC in terms of the dynamic response, tracking reference, precision, and THD of the injected currents into the grid under random wind speed.

The outcomes describe the robustness of the proposed MPPT technique using TOSMC combined with pitch angle control at different operating wind speed ranges, which enhances the efficiency of the power generation in the wind turbine system. As well as, the simulation study has confirmed that the Venturini modulation algorithm has high effectiveness in terms of the acceptable waveform, high transformation ratio (0.86), and simplicity of

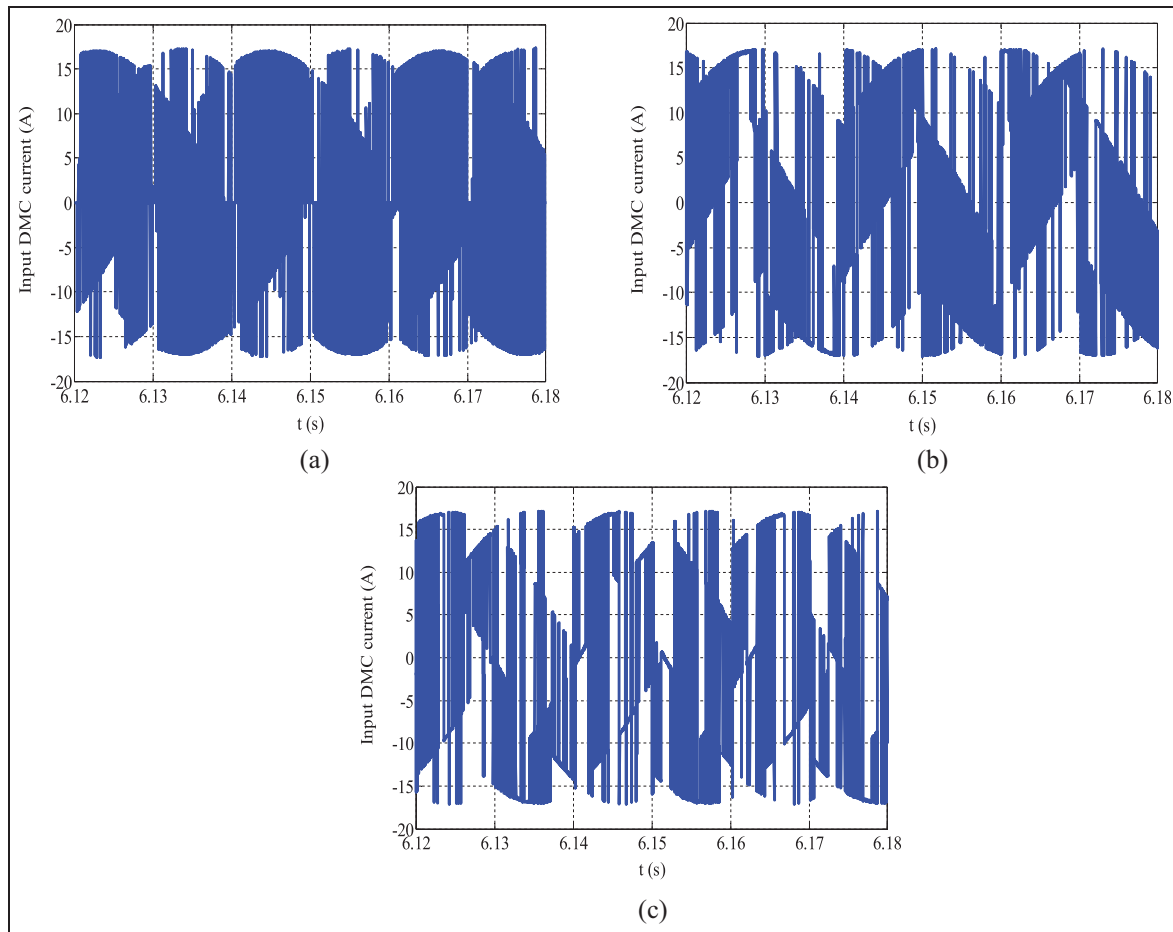


Figure 24. Input DMC current IA: (a) FOSMC, (b) SOMC, and (c) TOSMC.

Table 2. Comparative study between the proposed TOSMC strategy and other strategies of control.

Performance criteria	FOSMC	SOSMC	TOSMC
Reactive and active power tracking	Good	Good	Excellent
Minimization of reactive and active power ripples	Good	Good	Very good
Minimization of stator current ripples	Good	Good	Very good
Torque tracking	Good	Good	Excellent
Dynamic response	Medium	Medium	Fast
MPPT tracking	Good	Very good	Excellent
THD (%)	1.38% (<5%)	1.28% (<5%)	1.06% (<5%)
Quality of stator current	Good	Very good	Excellent
Performance	Medium	Medium	High

implementation. The use of a damped RLC passive filter combined with the direct matrix converter minimizes the rate of harmonics THD hence, it is possible to ensure a clean production of electrical energy from the wind turbine system.

Future research needs to focus on the control of the power converter, improving wind turbine system efficiency using developed control strategies and more efficient and robust. Furthermore, an experimental implementation of the proposed drive system can be accomplished.

Declaration of conflicting interests

The author(s) declared no potential conflicts of interest with respect to the research, authorship, and/or publication of this article.

Funding

The author(s) received no financial support for the research, authorship, and/or publication of this article.

ORCID iD

Amal Dendouga  <https://orcid.org/0000-0003-2202-2035>

References

- Adouni A, Chariag D, Diallo D, et al. (2016) FDI based on artificial neural network for low-voltage-ride-through in DFIG-based wind turbine. *ISA Transactions* 64: 353–364.
- Alhato MM and Bouallège S (2019) Direct power control optimization for doubly fed induction generator based wind turbine systems. *Mathematical and Computational Applications* 24(3): 77.
- Amrane F and Chaiba A (2016) Performances of type-2 fuzzy logic control and neuro-fuzzy control based on DPC for grid connected DFIG with fixed switching frequency. *International Journal of Electrical and Computer Engineering* 10(7): 870–878.
- Amrane F, Francois B and Chaiba A (2022) Experimental investigation of efficient and simple wind-turbine based on DFIG-direct power control using LCL-filter for stand-alone mode. *ISA Transactions* 125: 631–664.
- Aydogmus O, Boztas G and Celikel R (2022) Design and analysis of a flywheel energy storage system fed by matrix converter as a dynamic voltage restorer. *Energy* 238: 121687.
- Benamor A, Benchouia MT, Srairi K, et al. (2019) A new rooted tree optimization algorithm for indirect power control of wind turbine based on a doubly-fed induction generator. *ISA Transactions* 88: 296–306.
- Benbouhenni H and Bizon N (2021a) Third-order sliding mode applied to the direct field-oriented control of the asynchronous generator for variable-speed contra-rotating wind turbine generation systems. *Energies* 14(18): 5877.
- Benbouhenni H and Bizon N (2021b) A synergetic sliding mode controller applied to direct field-oriented control of induction generator-based variable speed dual-rotor wind turbines. *Energies* 14(15): 4437.
- Benbouzid M, Beltran B, Amirat Y, et al. (2014) Second-order sliding mode control for DFIG-based wind turbines fault ride-through capability enhancement. *ISA Transactions* 53: 827–833.
- Borlaug IG (2017) *Higher-order sliding mode control*. Master's Thesis, Norwegian University of Science and Technology, Norway.
- Bouar N, Labdai S and Boulkroune A (2019) PSO-GSA based fuzzy sliding mode controller for DFIG-based wind turbine. *ISA Transactions* 85: 177–188.
- Casadei D, Serra G, Tani A, et al. (2002) Matrix converter modulation strategies: A new general approach based on space-vector representation of the Switch State. *IRE Transactions on Industrial Electronics* 49(2): 370–381.
- Chaoui H, Hamane B and Doumbia ML (2016) Adaptive control of Venturini modulation based matrix converters using interval type-2 fuzzy sets. *Journal of Control Automation and Electrical Systems* 27: 132–143.
- Chojaa H, Derouich A, Chehaidia SE, et al. (2021) Integral sliding mode control for DFIG based WECS with MPPT based on artificial neural network under a real wind profile. *Energy Reports* 7: 4809–4824.
- El Mourabit Y, Aziz D, Abdelaziz EG, et al. (2019) Implementation and validation of backstepping control for PMSG wind turbine using dSPACE controller board. *Energy Reports* 5: 807–821. DOI: 10.1016/j.egy.2019.06.015.
- Dahbi A, Nait-Said N and Nait-Said MS (2016) A novel combined MPPT-pitch angle control for wide range variable speed wind turbine based on neural network. *International Journal of Hydrogen Energy* 41(22): 9427–9442.
- Dekali Z, Baghli L and Boumediene A (2021) Improved Super Twisting based high order direct power sliding mode control of a connected DFIG variable speed wind turbine. *Periodica Polytechnica Electrical Engineering and Computer Science* 65(4): 352–372.
- Dendouga A (2010) *Contrôle et uissances ctive t eactive de a achine a ouble limentation (DFIM)*. Batna: Thèse University of Batna.
- Dendouga A (2020) Conventional and second order sliding mode control of permanent magnet synchronous motor fed by Direct Matrix Converter: Comparative Study. *Energies* 13(19): 5093–1871.
- Dendouga A and Dendouga A (2019) High performance vector control of permanent magnet synchronous motor fed by direct SVM matrix converter. In: *2019 4th International conference on power electronics and their applications (ICPEA)*, Elazig, Turkey, 25–27 September, pp. 1–6. Available at: <https://ieeexplore.ieee.org/document/8911197>; <https://doi.org/10.1109/ICPEA1.2019.8911197> (accessed 25 November 2019).
- Dendouga A and Dendouga A (2022) A comparative study between the PI and SM controllers used by nonlinear control of induction motor fed by SVM matrix converter. *IETE Journal of Research* 68(4): 3019–3029.

- Djilali L, Sanchez EN and Belkheiri M (2020) First and high order sliding mode control of a DFIG-Based wind turbine. *Electric Power Components and Systems* 48: 105–116.
- Dursun EH and Kulaksiz AA (2020) Second-order sliding mode voltage-regulator for improving MPPT efficiency of PMSG-based WECS. *International Journal of Electrical Power & Energy Systems* 121: 106149.
- Hamane B, Doumbia ML, Chaoui H, et al. (2015) PI and RST control design and comparison for matrix converters using Venturini modulation strategy. *Journal of Power and Energy Engineering* 03(08): 36–54.
- Hamzaoui I, Bouchafaa F and Talha A (2016) Advanced control for wind energy conversion systems with flywheel storage dedicated to improving the quality of energy. *International Journal of Hydrogen Energy* 41(45): 20832–20846.
- Kaloi GS, Wang J and Baloch MH (2016) Active and reactive power control of the doubly fed induction generator based on wind energy conversion system. *Energy Reports* 2: 194–200.
- Kelkoul B and Boumediene A (2021) Stability analysis and study between classical sliding mode control (SMC) and super twisting algorithm (STA) for doubly fed induction generator (DFIG) under wind turbine. *Energy* 214: 118871.
- Khan MJ (2022) An AIPO MPPT controller based real time adaptive maximum power point tracking technique for wind turbine system. *ISA Transactions* 123: 492–504.
- Medjber A, Guessoum A, Belmili H, et al. (2016) New neural network and fuzzy logic controllers to monitor maximum power for wind energy conversion system. *Energy* 106(1): 137–146.
- Morshed MJ and Fekih A (2017) A new fault ride-through control for DFIG-based wind energy systems. *Electric Power Systems Research* 146: 258–269.
- Nguyen H, Nguyen TD and Lee H (2016) A modulation strategy to eliminate cmv for matrix converters with input power factor compensation. In: *IECON 2016 - 42nd annual conference of the IEEE Industrial Electronics Society*, Florence, Italy, 23–26 October, pp.6237–6242. New York, NY: IEEE. Available at: <https://ieeexplore.ieee.org/document/7793573>; <https://doi.org/10.1109/IECON.2016.7793573> (accessed 22 December 2016).
- Nguyen HN, Nguyen MK, Duong TD, et al. (2020) A study on input power factor compensation capability of Matrix Converters. *Electronics* 9(1): 82–18.
- Patel R, Hafiz F, Swain A, et al. (2021) Nonlinear rotor side converter control of DFIG based wind energy system. *Electric Power Systems Research* 198: 107358.
- Rezaei MM (2018) A nonlinear maximum power point tracking technique for DFIG-based wind energy conversion systems. *Engineering Science and Technology, an International Journal* 21(5): 901–908.
- Rodríguez J, Silva E, Blaabjerg F, et al. (2005) Matrix converter controlled with the direct transfer function approach: Analysis, modelling and simulation. *International Journal of Electronics* 92: 63–85.
- Saihi L, Berbaoui B, Glaoui H, et al. (2019) Robust sliding mode H_∞ controller of DFIG based on variable speed wind energy conversion system. *Periodica Polytechnica Electrical Engineering and Computer Science* 64(1): 53–63.
- Sami I, Ullah S, Ali Z, et al. (2020) A super twisting fractional order terminal sliding mode control for DFIG-based wind energy conversion system. *Energies* 13(9): 2158.
- She H, Lin H, Wang X, et al. (2010) Damped input filter design of matrix converter. In: *2009 International conference on power electronics and drive systems (PEDS)*, pp.672–677. New York, NY: IEEE. Available at: <https://ieeexplore.ieee.org/document/5385684>; <https://doi.org/10.1109/PEDS.2009.5385684> (accessed 19 January 2010).
- Soomro MA, Memon ZA, Kumar M, et al. (2021) Wind energy integration: Dynamic modeling and control of DFIG based on super twisting fractional order terminal sliding mode controller. *Energy Reports* 7: 6031–6043.
- Taraft S, Rekioua D, Aouzellag D, et al. (2015) A proposed strategy for power optimization of a wind energy conversion system connected to the grid. *Energy Conversion and Management* 101: 489–502.
- Venturini M and Alesina A (1980) The generalized transformer: A new bidirectional sinusoidal waveform frequency converter with continuously adjustable input power factor. In: *Proceedings of the IEEE power electronics specialists conference, PESC'80*, Atlanta, 16–20 June 1980, pp.242–252. Available at: <http://ieeexplore.ieee.org/stamp/stamp.jsp?tp=&number=7089455>
- Wang J, Bo D, Miao Q, et al. (2021) Maximum power point tracking control for a doubly fed induction generator wind energy conversion system based on multivariable adaptive super-twisting approach. *International Journal of Electrical Power & Energy Systems* 124: 106347.
- Yaichi I, Semmah A and Wira P (2019a) Direct power control of a wind turbine based on doubly fed induction generator. *European Journal of Electrical Engineering* 21(5): 457–464.
- Yaichi I, Semmah A, Wira P, et al. (2019b) Super-twisting sliding mode control of a doubly-fed induction generator based on the SVM Strategy. *Periodica Polytechnica Electrical Engineering and Computer Science* 63(3): 178–190.